



Ionic Liquid Additives in Water-Based Lubricants for Bearing Steel – Effect of Electrical Conductivity and pH on Surface Chemistry, Friction and Wear

W. Wijanarko^{1,2*}, H. Khanmohammadi¹ and N. Espallargas^{1*}

¹Norwegian Tribology Center, Department of Mechanical and Industrial Engineering, Norwegian University of Science and Technology (NTNU), Trondheim, Norway, ²Department of Mechanical Engineering, Sepuluh Nopember Institute of Technology (ITS), Surabaya, Indonesia

OPEN ACCESS

Edited by:

Jun Qu,
Oak Ridge National Laboratory (DOE),
United States

Reviewed by:

Anthony Somers,
Deakin University, Australia
Xin He,
Oak Ridge National Laboratory (DOE),
United States

*Correspondence:

W. Wijanarko
wahyu.wijanarko@ntnu.no
wijanarko@me.its.ac.id
N. Espallargas
nuria.espallargas@ntnu.no

Specialty section:

This article was submitted to
Tribology,
a section of the journal
Frontiers in Mechanical Engineering

Received: 11 August 2021

Accepted: 02 December 2021

Published: 04 January 2022

Citation:

Wijanarko W, Khanmohammadi H and
Espallargas N (2022) Ionic Liquid
Additives in Water-Based Lubricants
for Bearing Steel – Effect of Electrical
Conductivity and pH on Surface
Chemistry, Friction and Wear.
Front. Mech. Eng 7:756929.
doi: 10.3389/fmech.2021.756929

Water-based lubricants have the potential to become the largest environmentally friendly lubricants in applications such as electric vehicles and the newly emerging green technologies of the future due to their inherent low viscosity and cooling properties. In order to be environmentally acceptable (EAL), both base lubricants and additives should comply with biodegradability, non-toxicity, and non-bioaccumulation requirements. Additives for water-based lubricants should ideally be polar and soluble in water and, at the same time, should not increase the electrical conductivity to critical levels for corrosion. However, most additives used in synthetic or mineral oils are non-polar. Ionic liquids have recently gained attention as lubricant additives due to their high polarity, making them highly surface-active (i.e. high tendency to adsorb on metal surfaces). However, they are seen as highly corrosive for many metal alloys. In this work, a water-glycol lubricant containing two different ionic liquids has been investigated as a potential green lubricant for a bearing steel AISI 52100 with accurate control on electrical conductivity and pH. The selected ionic liquids were tributylmethylphosphonium dimethylphosphate (PP) and 1-butyl-1-methylpyrrolidinium tris(pentafluoroethyl)trifluorophosphate (BMP). The tribological behaviour of the ionic liquids was compared with a well-known organic friction modifier, dodecanoic acid (C12). The ionic liquids showed lower friction and wear rate than the water-based lubricant alone. However, they showed higher friction than the lubricant formulated with C12, in which PP gave lower friction than BMP due to low pH. A detailed subsurface analysis of the wear track using scanning-transmission electron microscopy (STEM) showed that a thick oxide tribofilm was built on the wear track for both lubricants formulated with ionic liquids due to high electrical conductivity. This tribofilm gave beneficial effect on wear. Although PP and BMP gave thicker tribofilms than C12, it was not durable, resulting in cracking and detachment.

Keywords: water-based lubricant, ionic liquids, pH, electrical conductivity, tribofilm

1 INTRODUCTION

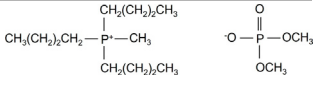
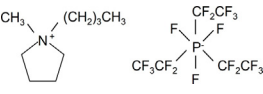
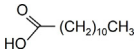
The production of electric vehicles (EVs) has grown in recent years. Ninety-eight EVs models were introduced to the market in 2019 compared to only two models available in 1997, and it is predicted to triple in 2025 (Transport and Environment, 2019; Chen et al., 2020). The EVs are considered as “green” vehicles compared to combustion engine vehicles (ICEVs) because they reduce the CO₂ emissions and other air pollutants (NO_x, carbon monoxide, unburnt hydrocarbons), which can reduce the global warming effect. According to the European Environment Agency data, the CO₂ emission of ICEVs is around 210 gCO₂/km, and it reduces to 70 gCO₂/km for EVs (European Environment Agency, 2019). In addition, the EVs have higher energy efficiency compared to ICEVs, in which EVs use up to 77% of total electric energy to drive the vehicle, whereas ICEVs only use up to 21% of total fuel energy (Holmberg and Erdemir, 2019). Similar to ICEVs, the components of EVs also need lubrication to operate in a tribological environment effectively. The tribological components of EVs will work at a higher speed than those in ICEVs, which makes the lubricant in EVs to function more as a torque transfer rather than as a load-bearing (Van Rensselar, 2019). The higher the speed of the tribological component, the higher the temperature generated in the lubricant. Because of that, the development of lubricants for EVs nowadays is moving towards low viscosity lubricants, which have better cooling properties and higher temperature stability (Narita and Takekawa, 2019).

Water-based lubricants are promising candidates as low viscosity lubricants for EV applications and others in which load-carrying capacity is not the main requirement. They have desirable properties such as better cooling ability, low toxicity, and fire resistance. Therefore, water-based lubricants are nowadays already used as an alternative to petroleum-based lubricants in applications such as hydraulic fluids (Tomala et al., 2010), cooling fluids for metal cutting (Khan et al., 2021), and bearings of the stern tubes in propeller shafts of ships (Huang et al., 2019). Moreover, water-based lubricants are used to mimic the body fluids to perform *in vitro* studies of the corrosion and tribocorrosion behaviour of bearing implant materials such as CoCrMo (Espallargas et al., 2015). However, water-based lubricants in many current applications have several drawbacks, such as high pour point, poor corrosion protection, high polarity (competing with additives for surface sites), and low viscosity (in cases when load-carrying capacity is needed), leading to poor lubricating performance as compared with mineral or synthetic oils. Therefore, the uncertainty in the tribological performance of water-based lubricants might hinder their application in EVs. There are some strategies to overcome the main drawbacks of water, such as using glycols (or similar substances) to increase the viscosity and decrease its pour point. In addition to glycols, the use of other additives to enhance the tribological performance (e.g. friction and wear) of water is a must (Tomala et al., 2010). Short-chain friction modifiers such as organic friction modifiers (OFMs) are typically used in water-glycol hydraulic fluids (Spikes, 2015; Bernat et al., 2018a; Bernat et al., 2018b). Other additives such as antiwear

(AW) or extreme pressure additives can also be used for water-based lubricants in case the application requires it (Chang et al., 2011). AW additives usually contain active elements such as phosphorus (P), sulphur (S), or halogens. One commonly used antiwear additive in petroleum-based lubricants is zinc dialkylthiophosphate (ZDDP). It was initially developed in the 1940s as an antioxidant, but soon it showed antiwear and corrosion inhibition properties for engine oils (Spikes, 2004; Nicholls et al., 2005). Even though ZDDP has several advantages as lubricant additive for engine oils however, in the recent years attempts to find alternatives to it have begun due to environmental issues. ZDDP is aquatically toxic, and it is an issue in environmentally sensitive applications like forestry, marine, etc. (Canter, 2019). Therefore, this additive is not suitable for environmentally friendly lubricant formulations. ZDDP contains zinc that generates ash upon combustion, resulting in degradation of the catalysts systems in cars. It is believed that the sulphur and phosphorus oxide together with the metallic ashes block the exhaust giving a rise in carbon monoxide and hydrocarbon emissions from the engine (Spikes, 2008). Therefore, in the case of oils for ICEVs the need to reduce the amount of sulphated ash, phosphorus, and sulphur (referred as SAPS) has become crucial. Indeed, the main metallic source for sulphated ash is zinc, which is present in ZDDP. And also, several governments have regulated the concentration limit of P and S in lubricants for ICEVs (THE EUROPEAN COMMISSION, 2014). Therefore, the need for more environmentally friendly additives has boosted the development and study of metallic-free or ashless additives with low or no P and S content as alternative to ZDDP. Worth noticing is that not all forms of phosphorous (P) and sulphur (S) are toxic to the environment, therefore the regulations limit the use of P and S in lubricant formulations, but not fully ban them (Candelaria, 2018).

Ionic liquids (ILs) are organic salts with a low melting point (below 100°C), consisting of anions and cations. ILs are attractive compounds due to their unique properties, such as low volatility, high thermal stability, and non-flammability (Seddon, 1997; Welton, 1999; Wasserscheid and Welton, 2002). They were used for the first time in the 1910s as a need to have salts at room temperatures. In the 1980s, they were “re-discovered” to be used as solvents in chemical reactions. Since then, they have been considered environmentally friendly substances for “green chemistry,” although there is some controversy around this topic (Welton, 2018). One of the many applications that boosted in the early 2000s for ILs was their use as high-performance lubricants (Ye et al., 2001; Liu et al., 2002). ILs are considered attractive lubricants because they tend to adsorb very effectively on surfaces (Somers et al., 2013). Therefore, ILs have been studied as neat lubricants but also as additives (Minami, 2009; Somers et al., 2013; Amiril et al., 2017; Xiao, 2017; Zhou and Qu, 2017). ILs as additives in water-based lubricants might be disadvantageous due to their ionic nature (i.e. corrosion attacks in metals). Therefore most studies of ILs as additives in water-based lubricants have focused on ceramic-on-ceramic contacts (Phillips and Zabinski, 2004; Xie et al., 2009) or non-halogenated ILs (Zheng et al., 2017; Wang et al., 2018; Dong et al., 2020). However, recent work in our group has shown that

TABLE 1 | Chemical formula, density, and chemical structure of all additives.

Abbr	Chemical name	Chemical formula	Density (g/cm ³)	Chemical structure
PP	Tributylmethylphosphonium dimethylphosphate	C ₁₅ H ₃₆ O ₄ P ₂	1.004	
BMP	1-butyl-1-methylpyrrolidinium tris(pentafluoroethyl) trifluorophosphate	C ₁₅ H ₂₀ F ₁₈ NP	1.647	
C12	Dodecanoic acid	CH ₃ (CH ₂) ₁₀ COOH	1.007	

halogenated ILs as additives in water-glycol form an efficient tribofilm that reduces friction and wear in stainless steel sliding against alumina (Khanmohammadi et al., 2020).

This work aims to investigate the viability of ILs as lubricant additives for low corrosion-resistant alloys such as bearing steel. The focus will be on corrosion resistance (controlling electrical conductivity and pH) and friction and wear performance. Two ILs (tributylmethylphosphonium dimethylphosphate and 1-butyl-1-methylpyrrolidinium tris(pentafluoroethyl) trifluorophosphate) have been investigated in a water-glycol lubricant. No anticorrosion additives (or any other) were used with the aim of studying the effect of ILs alone. An OFM, dodecanoic acid, was used as a reference.

2 MATERIALS AND METHODS

Materials

AISI 52100 bearing steel, purchased from Smith Stål (Trondheim, Norway), was chosen as the test material. Sample disks were prepared by cutting the 30 mm diameter steel rod with a thickness of 6 mm. The samples were ground using a resin-bonded diamond disk, subsequently polished using 9, 6, and 3 μm diamond suspensions. The polished samples were ultrasonically cleaned in distilled water-ethanol mixture (ca. 1:1) for 5 min, then rinsed with fresh ethanol and dried with pressurized air. The base lubricant was prepared by mixing water with glycol in a 1:1 proportion (abbreviated WG). Two ionic liquids (ILs) were used as additives in WG, i.e. tributylmethylphosphonium dimethylphosphate (abbreviated PP) and 1-butyl-1-methylpyrrolidinium tris(pentafluoroethyl) trifluorophosphate (abbreviated BMP). The tribological behaviour was compared with an organic friction modifier, i.e. dodecanoic acid (abbreviated C12). Glycol (≥99% purity) and PP (97%) were purchased from Acros Organics and Fluorochem, respectively. Meanwhile, both BMP (≥98%) and C12 (≥99%) were purchased from Sigma-Aldrich. All chemicals were used as received. The chemical formula, density, and chemical structure of all additives used in this work are shown in **Table 1**. In an independent study performed in our research group, ILs in the same base lubricant had been tested at different concentrations (0.25, 0.5, 1, 2, and 4 wt %). It was found that ILs were fully soluble at all concentrations, however the friction was stable only at concentrations equal and above 1 wt%, therefore 1 wt% was

selected as the concentration for ILs. In the case of C12, a previous study conducted in our research group showed that 0.1 wt% is the optimal concentration for C12 in water glycol lubricant, therefore 0.1 wt% of C12 was chosen as the reference lubricant for the present work (Bernat et al., 2018b). The base lubricant and additives were mixed using magnetic stirring for 4 h at 50°C. The lubricant was continuously stirred at room temperature for 20 h before being used.

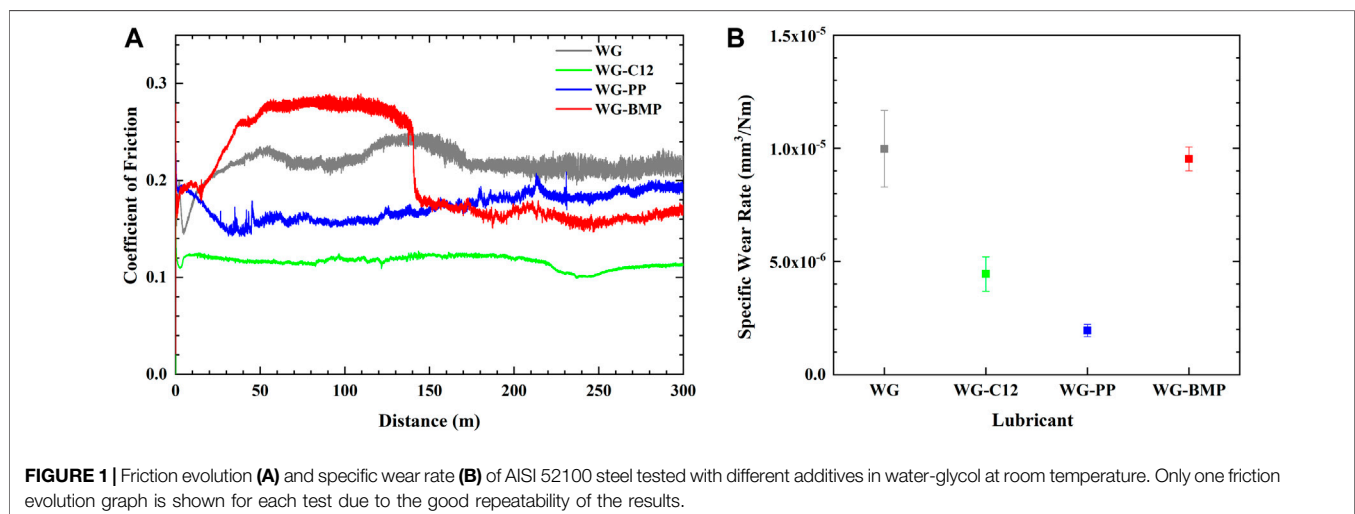
Testing and Characterization Methods

The density of the lubricants was measured by the constant fluid volume weighing method. The dynamic viscosity at 23°C in humid air was measured using a rheometer (Haake Mars Rotational Rheometer with a CC27 cylinder measuring system, with the built-in Peltier element). The electrical conductivity of the lubricants was measured using a conductivity meter (Hanna Instruments HI-2300). The pH of the lubricant was measured using a pH meter (Hanna Instruments HI-2210). The open circuit potential (OCP) was measured for 4 h using a Gamry Interface 1000 Potentiostat with Ag/AgCl KCl saturated reference electrode. Friction and wear were measured using a rotating ball-on-disk tribometer (Phoenix tribology). In this test, a stationary alumina ball, purchased from Precision Ball and Gauge Co. Ltd., was in contact with the flat AISI 52100 disk using a dead weight in the presence of the lubricants at room temperature. The diameter of the alumina ball was 6 mm, and the normal load applied was 20 N, resulting in an initial maximum Hertzian contact pressure of 1.96 GPa. The disk's rotation speed and the track diameter were set to 40 rpm and 10 mm, respectively, which gave a sliding speed of 2.09 cm/s. The calculated EHL Hamrock-Dowson lambda (λ) value is 0.016, indicating boundary lubrication conditions. The additives have only a slight effect on the dynamic viscosity of the lubricant. As a result, the λ value still meets the boundary lubrication conditions. At least two tests were performed for each condition to verify the repeatability of the results.

Alicona Infinite Focus optical 3D microscope and MountainsMap software were used to quantify the wear volume from four different locations of the wear track. Archard's equation was used to calculate the average specific wear rate (SWR) from two samples for each condition (Archard, 1953). The average SWR value and the standard deviation were reported.

TABLE 2 | Detailed curve-fitting parameters of compounds used for XPS characterization.

Signal	Binding energy (± 0.1 eV)	FWHM (± 0.1 eV)	Line shape	Assignment	References
Fe 2p	712.8	2.9	GL (30)	Fe ³⁺	Fredriksson et al. (2012), Viesca et al. (2013), Zavieh and Espallargas (2017)
	712.6	2.9	GL (30)	FePO ₄	
	711.0	2.9	GL (30)	Fe ₃ O ₄	
	709.5	2.9	GL (30)	FeO	
	706.8	0.9	LF (0.8,2,20,0)	Fe 2p _{3/2}	
F 1s	684.9	1.6	GL (30)	F ⁻	Yu et al. (2008), Viesca et al. (2013)
Cr 2p	578.7	1.5	GL (30)	CrO ₃	Fredriksson et al. (2012), Zavieh and Espallargas (2017)
	577.3	1.5	GL (30)	Cr(OH) ₃	
	576.1	1.5	GL (30)	Cr ₂ O ₃	
	573.9	1.2	LF (0.8,2,8,0)	Cr 2p _{3/2}	
O 1s	531.6	1.8	GL (30)	O-H	Zavieh and Espallargas (2017), Long et al. (2019)
	530.5	1.1	GL (30)	O-M	
P 2p	133.7	1.6	GL (30)	(PO ₄ ³⁻)	Rokosz et al. (2016), Urtis et al. (2019)



FEI Helios Nanolab DualBeam focused ion beam and scanning electron microscopy (SEM-FIB) was used to study the surface and cross-section of the wear tracks. Platinum or carbon was deposited on the wear track surface to protect it from the milling and polishing processes. Deposition, milling, and polishing were carried out using a Gallium ion source. The secondary electron images of the wear track surface and cross-section were taken using the Everhart-Thornley detector (ETD) and through lens detector (TLD), respectively. The SEM-FIB was also used to prepare thin wear track lamellae with thickness less than 60 nm. The lamellae were examined by scanning-transmission electron microscopy (STEM, Hitachi SU9000) equipped with an x-ray energy dispersive spectroscopy (EDS) detector (Ultim Extreme, Oxford Instruments).

The elemental composition of the wear tracks was studied by x-ray photoelectron spectroscopy (XPS) (Kratos Axis Ultra DLD machine). A monochromatic Al K α was used as the x-ray source with accelerating voltage and current of 10 kV and 10 mA, respectively. Electrostatic lens mode was selected to collect the elemental data during acquisitions with a 9×10^{-9} Torr chamber pressure. The

elemental map was collected using survey acquisition with a pass energy of 160 eV and a step size of 1 eV. From the survey acquisition results, iron (Fe), chromium (Cr), oxygen (O), phosphorus (P), and fluorine (F) were selected for the high-resolution scan with a pass energy of 20 eV and a step size of 0.1 eV. Elemental data acquisition below the surface was performed by milling the surface using Argon ions at a pressure of 4.4×10^{-7} Torr, an energy of 4 kV, and a raster size of 2.5×2.5 mm. The sputtering rate was calibrated using tantalum oxide (Ta₂O₅) of known thickness, resulting in a 2 nm/min sputtering rate. CasaXPS software was used to fit the curves with the curve-fitting parameters (Table 2) for evaluation and quantification.

3 RESULTS

Tribological Testing

The friction evolution and specific wear rate of the AISI 52100 steel sliding against alumina in the presence of all lubricants are presented in Figure 1. The coefficient of friction (COF) of WG

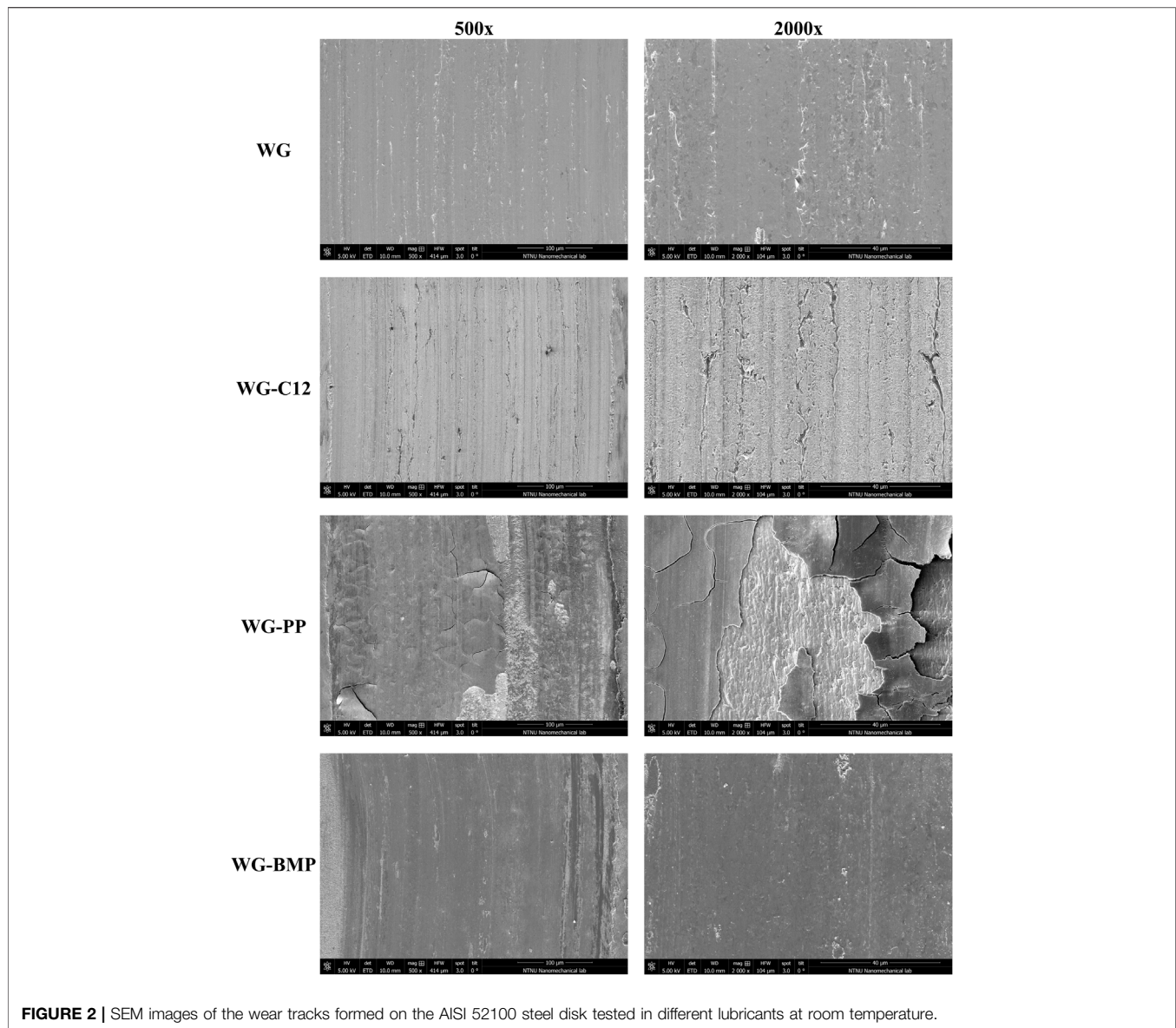


FIGURE 2 | SEM images of the wear tracks formed on the AISI 52100 steel disk tested in different lubricants at room temperature.

alone shows a value of 0.21 after the running-in period and slightly fluctuates for the rest of the test. The base lubricant with dodecanoic acid (WG-C12) shows a short running-in period and stabilizes at values between 0.10 and 0.12. The addition of 1 wt% PP to the base lubricant (WG-PP) shows a COF of 0.16 during the running-in period, followed by a steady increase to 0.19 at the end of the test. The friction evolution of BMP-containing lubricant (WG-BMP) shows two distinct regions: a COF of 0.28 after the running-in period during 100 m of sliding, followed by an abrupt drop to 0.18 until the end of the test. For wear, the base lubricant generates the highest wear rate of $9.98 \times 10^{-6} \text{ mm}^3/\text{Nm}$, followed by BMP, C12, and PP with wear rates of 9.53×10^{-6} , 4.45×10^{-6} , and $1.95 \times 10^{-6} \text{ mm}^3/\text{Nm}$, respectively.

Wear Track Morphology

Figure 2 shows the SEM images of the wear tracks' surface at two different magnifications. The wear track of the sample tested with

base lubricant only shows a smooth surface with little sign of plastic deformation. The wear track of the sample tested with WG-C12 is not as smooth as the base lubricant alone, and some surface cracks are observed. The wear track morphology is utterly different for WG-PP, in which many cracks are observed, resulting in detachments in some areas. The wear track of the sample tested with WG-BMP shows a smooth surface with no signs of plastic deformation.

SEM-FIB was used to investigate the wear track cross-section, as shown in **Figure 3**. The length of the cross-section was $20 \mu\text{m}$ and was taken from the centre of the wear track and perpendicular to the sliding direction. Different degrees of recrystallization and plastic deformation are observed. Samples lubricated with base lubricant alone show a high degree of recrystallization and plastic deformation due to the high friction. The addition of C12 to the base lubricant (which reduced the coefficient of friction by 50%) results in a lower

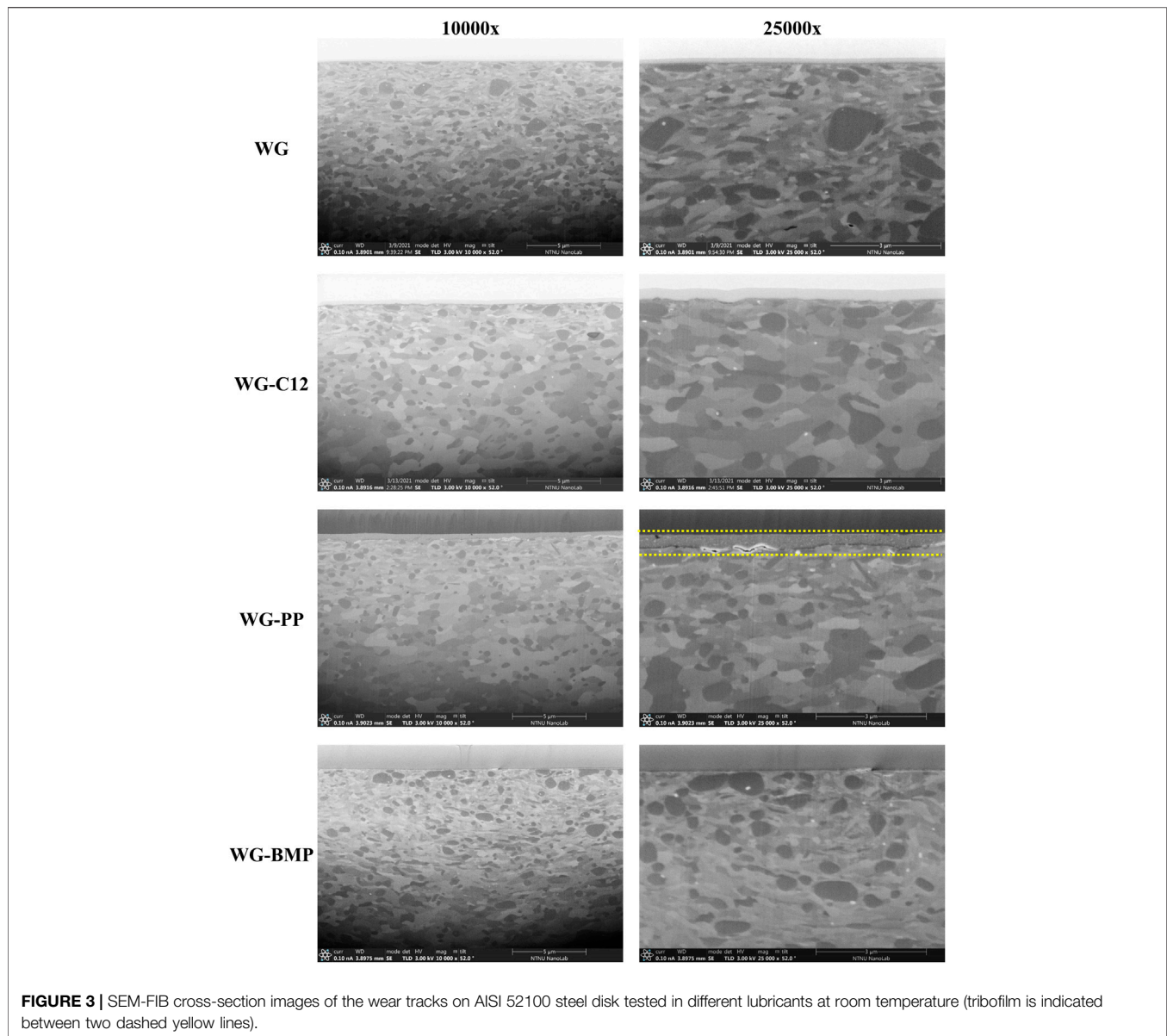


FIGURE 3 | SEM-FIB cross-section images of the wear tracks on AISI 52100 steel disk tested in different lubricants at room temperature (tribofilm is indicated between two dashed yellow lines).

degree of recrystallization and plastic deformation and in a rougher surface that is in agreement with the view of the wear track surface (**Figure 2**). In the WG-BMP sample, the degree of recrystallization and plastic deformation are in between WG and WG-C12. However, the WG-PP sample shows a lower degree of recrystallization and plastic deformation, despite the high coefficient of friction. Interestingly, the top surface of the WG-PP sample is clearly covered by a thick layer (tribofilm), which might be responsible for the lower recrystallization and plastic deformation.

For the WG-BMP sample, a new test was performed for 100 m before the drop in friction is observed (**Figure 1A**) to analyse this abrupt transition on friction evolution. The top view and cross-section images of the WG-BMP 100 m sample wear track are shown in **Figure 4**, along with the WG-BMP 300 m sample for comparison. The WG-BMP 100 m sample wear track shows wear

marks, surface cracks, and plastic deformation, whereas a smooth surface without wear marks is observed for the WG-BMP 300 m sample. These wear surface morphologies are in agreement with the friction evolution (**Figure 1A**), where rougher surfaces produced higher friction and vice versa. Despite having higher friction, the test performed at 100 m resulted in lower recrystallization and plastic deformation than the test at 300 m due to a thick tribofilm formed on the surface, as similarly observed for WG-PP (**Figure 3**).

Tribofilm Characterization

In order to investigate the tribofilms, the cross-section of all samples was examined by STEM. A thin lamella of 60 nm from each sample was prepared using SEM-FIB. The STEM images and the EDS elemental mapping are presented in **Figure 5**. The chosen elements for mapping are oxygen, iron, chromium,

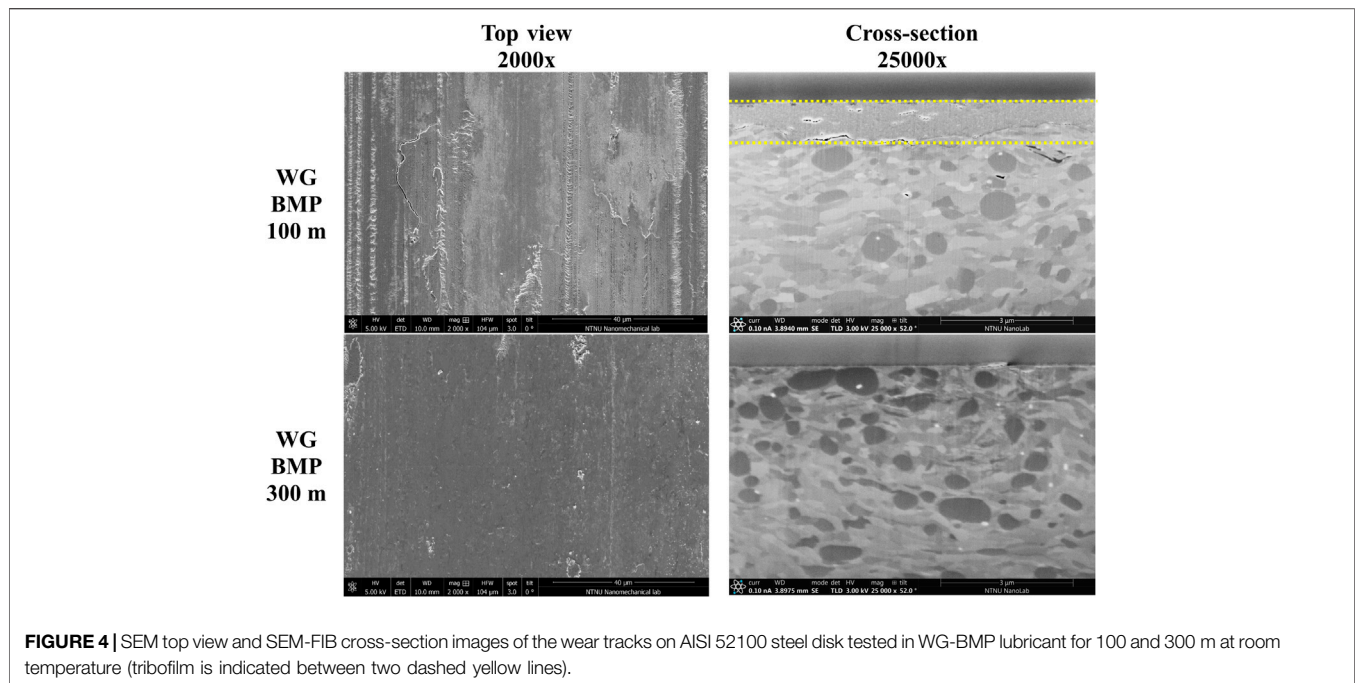


FIGURE 4 | SEM top view and SEM-FIB cross-section images of the wear tracks on AISI 52100 steel disk tested in WG-BMP lubricant for 100 and 300 m at room temperature (tribofilm is indicated between two dashed yellow lines).

and phosphorous, which are present in the bulk material AISI 52100 steel and the ILs. The oxygen is an indicator of the presence of oxides. Although BMP contains fluorine, this element was not selected for EDS mapping due to the close F K α and Fe L α energy. A platinum protective layer was deposited before the FIB milling processes for WG and WG-C12 samples. For WG-PP and WG-BMP samples, carbon was used as a protective layer instead of platinum to provide better mapping contrast because Pt M α and P K α energies are close to each other.

As seen from the STEM images, the sample lubricated with WG alone shows a thin tribofilm on the surface with a thickness of less than 10 nm (measured from higher magnification images). The lack of additives could be the reason for this thin tribofilm. The WG-C12 sample shows a slightly thicker tribofilm detected on the surface with a ca. 20 nm thickness. A very thick tribofilm is observed for the WG-PP sample of 400–900 nm thickness. In addition, wear debris is observed in the tribofilm, as indicated from the STEM and Fe mapping images. The tribofilm is not fully adhered to the base material, as indicated by a crack at the interface with the base material. Similar characteristics, such as thick tribofilm, wear debris inside the tribofilm, and crack at the interface with the base material, are also observed for the WG-BMP 100 m sample. The thickness of the tribofilm is ca. 600–1,300 nm. For WG-BMP 300 m sample, there is only a tribofilm with a thickness of less than 20 nm observed. EDS mapping of the cross-sections shows high oxygen levels in the tribofilms of all samples, indicating they consist mainly of oxides. Only an additional element, phosphorous, is detected in the WG-PP sample.

Point EDS analysis was performed to get a detailed chemical composition of the tribofilm from each sample, and the results are shown in **Table 3** along with the tribofilm thickness after STEM. The point analysis shows mostly Fe and O, as already seen with the mapping (**Figure 5**). Chromium is not detected in the

tribofilms since it is mainly found as chromium carbide precipitate (**Figure 5**).

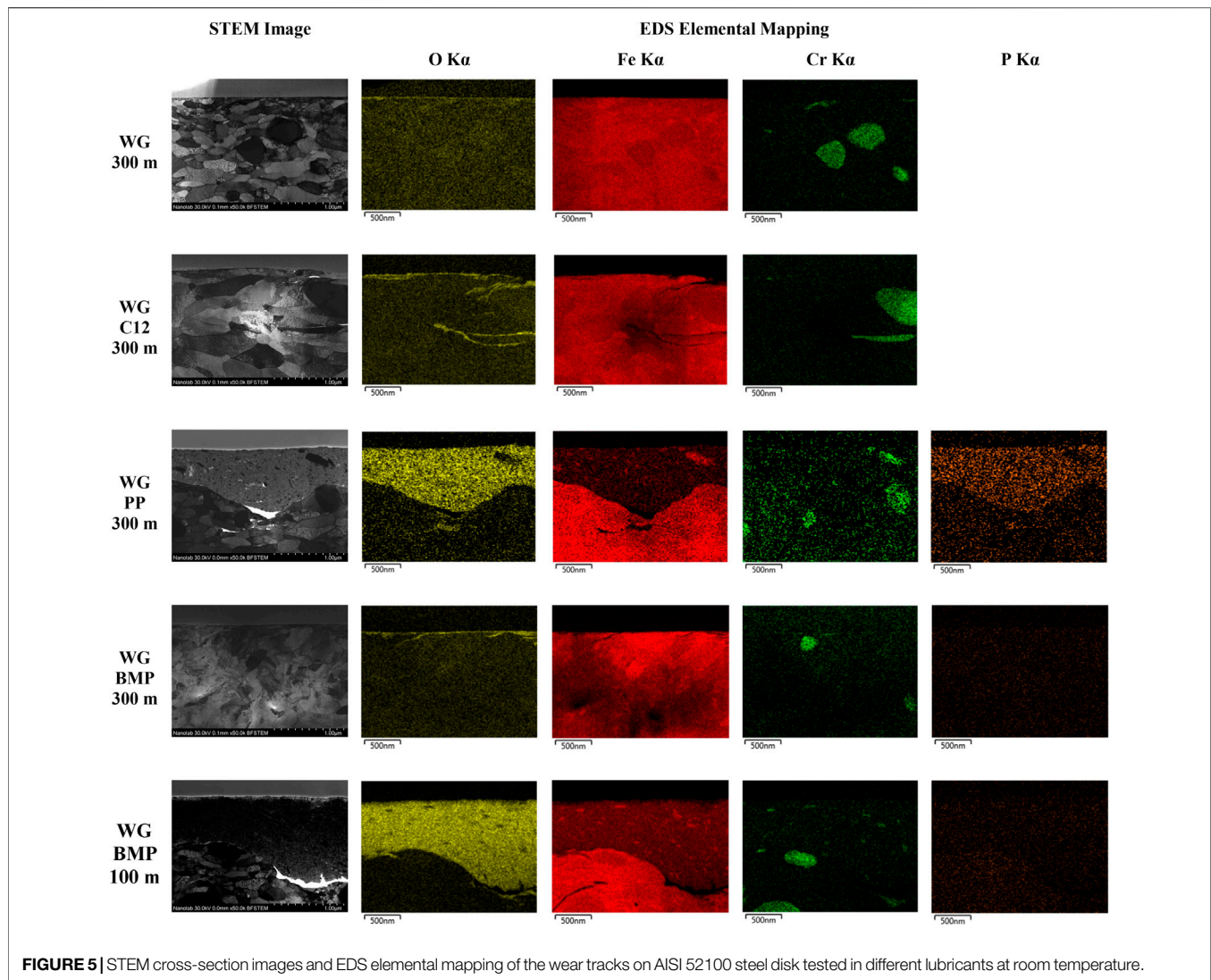
Surface chemical analysis inside the wear tracks was studied by x-ray photoelectron spectroscopy (XPS) for WG-PP 300 m, WG-BMP 300 m, and WG-BMP 100 m samples only. These three samples were selected to evaluate more in detail the chemical bonding states of phosphorous and fluorine because these elements were difficult to detect with EDS. The XPS analysis was done by sputtering the wear track with Argon for 300 s (ca. 10 nm depth), reaching half of the tribofilm in WG-BMP 300 m and the top surface of the WG-PP 300 m and WG-BMP 100 m tribofilms. The detailed XPS spectra are shown in **Figure 6**.

The results show the presence of Fe only, and no Cr was found. Deconvolution of the Fe spectra shows that they consist of Fe metal (Fe⁰), Fe oxides (FeO, Fe₃O₄, Fe₂O₃), FePO₄, and Fe hydroxides (FeOOH, Fe(OH)₃). The Fe⁰ percentage in WG-PP is higher than in WG-BMP 300 m even though the depth of analysis is far from the bulk material (minimum ca 380 nm from the bulk). This can be due to wear debris spreading in the tribofilm (**Figure 5**) or due to the large tribofilm detachment areas (**Figure 4**). The O spectra show mostly metal hydroxide and metal oxide, in agreement with the Fe spectra. Phosphate (PO₄)³⁻ is detected from the Fe2p and P2p spectra in the case of WG-PP, which is in agreement with the EDS analysis (**Figure 5**). In the case of WG-BMP (both 100 and 300 m), no P and F are detected in the tribofilm, and only oxides and hydroxides are present.

4 DISCUSSION

Chemical Effects on the Tribofilm Formation

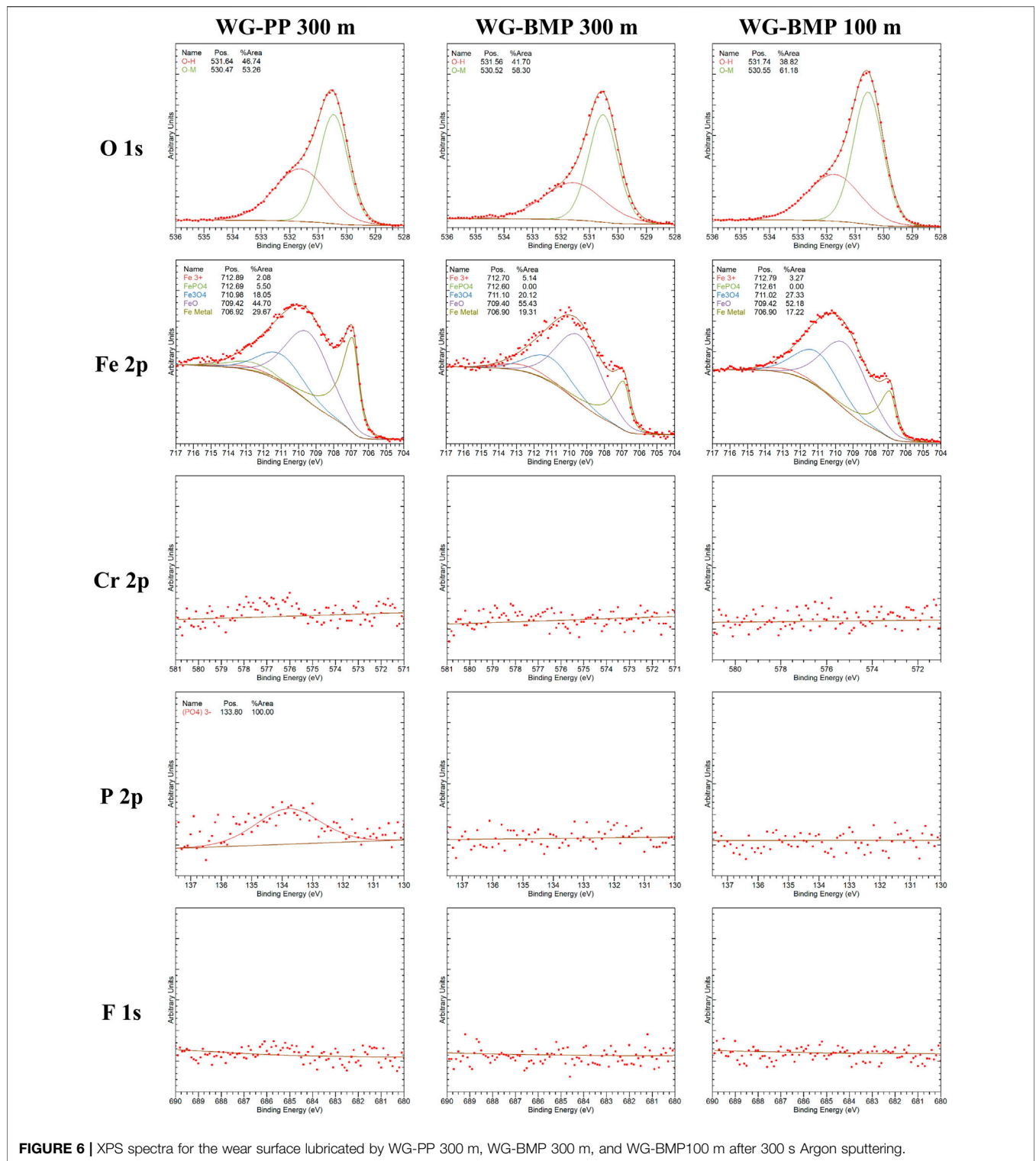
The tribofilm formation is influenced by several factors, such as lubricant chemical composition, contact mechanics,

**TABLE 3** | Relative concentration inside the tribofilm (at%).

Sample	Tribofilm thickness (nm)	Elemental concentration in tribofilm (at%)			
		Fe	Cr	O	P
WG 300 m	<10	57.81	0.00	42.19	–
WG-C12 300 m	20	42.60	0.00	57.40	–
WG-PP 300 m	400 – 900	29.46	0.00	64.60	5.94
WG-BMP 300 m	20	49.67	0.00	50.33	0.00
WG-BMP 100 m	600 – 1,300	44.82	0.00	55.18	0.00

environment, and types of materials (Kapsa and Martin, 1982; Morina and Neville, 2007; Jacobson et al., 2010). In this work, the lubricant chemical composition was varied by adding different ionic liquids to the base lubricant to study the effect of electrical conductivity and pH on tribofilm formation, friction and wear. **Table 4** shows the different physical and chemical characteristics of all the lubricant-additive mixtures studied in this work.

The electrical conductivity of the lubricant slightly increases when adding C12. However, it increases by two orders of magnitude when adding the ionic liquids, but it is still below the electrical conductivity of tap water. Of the two ILs, PP results in the highest electrical conductivity (twice higher than BMP). PP and BMP increases the electrical conductivity of the based lubricant due to the nature of the ionic liquid which act as a charge carrier inside the lubricant. The higher molecular weight



of BMP can be the reason for its lower electrical conductivity compared to PP in water media. C12 and PP decrease the pH to acidic values. The deprotonation of the carboxylic group (COOH) is the main reason for the drop of pH in this case. In the case of PP, the possible formation of phosphoric acid is the

reason for dropping in pH due to the ionic interaction between the cation or the anion of PP with water. However, BMP keeps the pH value of the base lubricant possibility due to the low electrical conductivity and therefore the lower interaction of the anions and cations with water as compared to PP. The OCP of the metal was,

TABLE 4 | Physical and chemical properties of all lubricants.

Lubricant	Additive concentration (wt%)	Density (g/cm ³)	Dynamic viscosity (mPa.s)	Electrical conductivity (μS/cm) ^a	pH	OCP vs Ag/AgCl (mV)
WG	—	1.040	13.99	2.5	7.3	-537
WG-C12	0.1	1.041	13.53	4.3	4.7	-396
WG-PP	1	1.039	13.76	211.2	3.4	-588
WG-BMP	1	1.045	14.02	109.3	7.0	-522

^aFor comparison, the electrical conductivity of tap water is ca 500 μS/cm and for seawater is ca 5,000 μS/cm.

TABLE 5 | Wear track chemical composition after XPS analysis.

Sample	Tribofilm thickness (nm) (after STEM from Table 3)	XPS chemical analysis (at%)				
		Fe ⁰	FeO	Fe ₃ O ₄	FePO ₄	Fe oxides/Fe ⁰ ratio
WG 300 m	<10			Not measured		
WG-C12 300 m	20			Not measured		
WG-PP 300 m	400–900	29.67	44.70	18.05	5.50	2.11
WG-BMP 300 m	20	19.31	55.43	20.12	0	3.91
WG-BMP 100 m	600–1,300	17.22	52.18	27.33	0	4.62

in all cases, around -500 mV, whereas it was only 100 mV more positive (ca. -400 mV) for C12. These OCP values are well in agreement with carbon steel exposed to water media and represent an active dissolution corrosion process (Fontana, 1987).

The differences in pH and electrical conductivity have an effect on the chemistry of the metal surface and, therefore, on the tribofilm formation. In **Table 5**, the chemical composition of the tribofilms obtained from XPS analysis is shown, along with the Fe oxides to metal ratio and tribofilm thicknesses. The lowest electrical conductivity leads to thin tribofilm formation (WG and WG-C12). Likewise, the highest electrical conductivity results in thicker tribofilms (WG-PP and WG-BMP 100 m). The tribofilm thickness only increases significantly if the electrical conductivity is high enough (**Table 5**). The Fe oxides to metal ratio is an indicator of the relative number of oxides inside the tribofilm. The sample lubricated with WG-PP shows the lowest Fe oxides to metal ratio (2.11). In the case of WG-BMP 300 m and WG-BMP 100 m the ratio increases to 3.91 and 4.62, respectively, indicating BMP produced more oxide compared to PP.

Based on the pH values (**Table 4**), it can be expected that in an acidic medium such as WG-PP (pH of 3.4) carbon steel would undergo iron dissolution compared to the medium with neutral pH (WG-BMP, pH of 7.0). Indeed, it was found by XPS (**Table 5**) that the WG-BMP 100 m has more oxides to metal ratio compared to WG-PP, however WG-PP had FePO₄ in addition to oxides. These two additives yielded a very thick tribofilm with very different chemical compositions (**Table 5**). The different tribological responses: WG-PP showed lower friction and wear rate than WG-BMP (**Figure 1**). Therefore, iron oxides and FePO₄ together have a more beneficial effect than iron oxides alone in the tribofilm. This is clearly seen by the friction evolution of WG-BMP in the first 150 sliding meters of the test, which is twice higher than in the last sliding meters. Once the iron oxide

tribofilm has been removed, its build-up is very slowly decreasing friction. In the case of WG-PP, friction is low throughout the test due to the presence of phosphates. However, this is not enough to reach the lowest friction values of WG-C12, since in this case, the friction mechanism is controlled by surface adsorption and not by tribofilm formation.

Unlike ZDDP, which has a metal atom in its structure, PP and BMP require external metal supply to grow a tribofilm. The source of the metal should come from the nascent base metal surface or the wear debris. Tribofilm formation consists of three stages, i.e. tribofilm initiation, wear debris generation and breakdown, and tribofilm growth (Zhou et al., 2017). Tribofilm initiation occurs when the lubricant reacts with the nascent metal surface to form a thin oxide film. This oxide film acts as an interlayer, providing a good bonding between the metal surface and the tribofilm, or acting as a barrier hindering further tribofilm growth (Stachowiak and Batchelor, 2014; Zhou et al., 2017). In the second stage, the material is removed from the top metal surface, generating wear debris, which reacts with the lubricant (i.e. oxidizes). Some of the wear debris gets trapped in the contact area, where it grinds and breaks down in nanosized particles. In the third stage, the tribofilm growth can occur via three mechanisms, i.e. mechanical deposition, chemical deposition, and oxygen diffusion (Zhou et al., 2017). In this work, the thick tribofilms found in WG-PP and WG-BMP 100 m have grown up via mechanical deposition and compacting of the wear debris nanoparticles in the contact area. This is clearly seen in **Figure 5** and later confirmed from the XPS analysis (**Figure 6** and **Table 5**), where iron oxides, iron phosphate and metallic iron are found in the tribofilms (at 10 nm from the surface). In addition, chemical deposition and oxygen diffusion have occurred, resulting in the formation of iron oxide and/or iron phosphate compounds in the tribofilm, leading to further tribofilm growth.

In this work, the electrical conductivity has controlled the tribofilm growth after the first stage of tribofilm formation. This is clear when looking at WG and WG-C12, where the first stage thin oxide film builds on the surface (Table 5) however, due to the low electrical conductivity, the dissolution of this oxide film is slower and hinders further wear debris deposition. Moreover, in the case of WG-C12, not only the thin oxide film is present on the surface, but also dodecanoic acid is strongly adsorbed providing low shear and preventing further tribofilm growth. For WG-PP and WG-BMP, the dissolution of the first stage thin oxide film takes place due to the high electrical conductivity providing active metal surface sites for wear debris deposition, facilitating further tribofilm build up.

The Effect of Tribofilm Formation on Friction Evolution

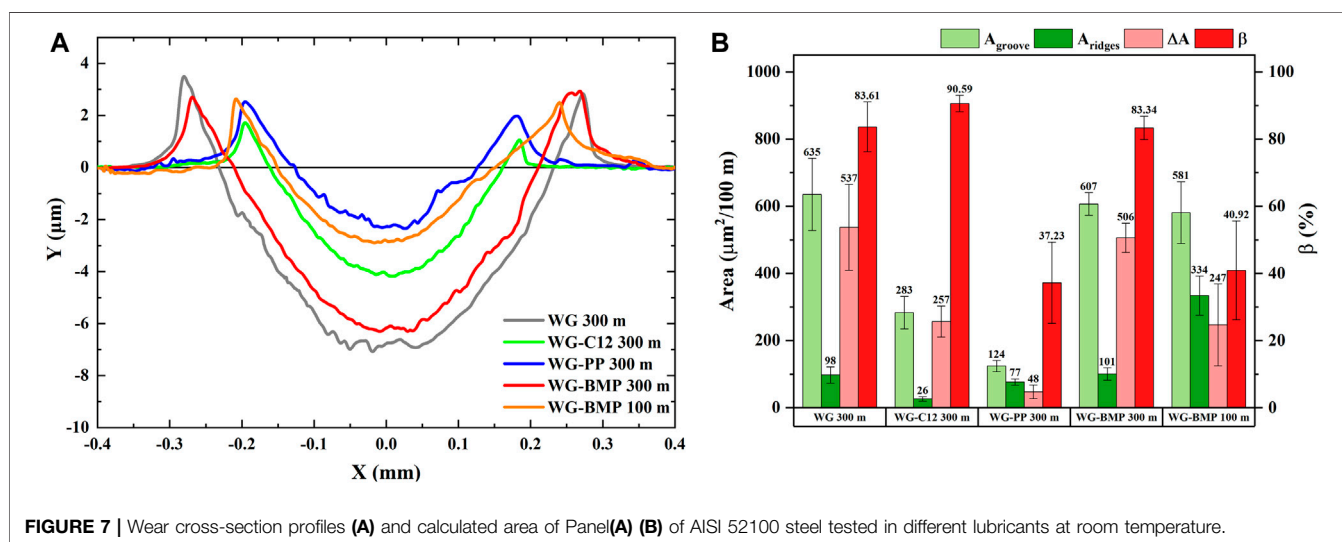
As shown in Figure 1, the friction evolution of WG alone was the highest, and by adding C12, the friction reduces drastically. According to the literature, the friction reduction of carboxylic acid in polar media is due to the thin oxide film formation and the adsorption of carboxylic acid onto the rubbing surface (Zavieh and Espallargas, 2017; Bernat et al., 2018b). Furthermore, a quartz crystal microbalance (QCM) study showed that carboxylic acid forms adsorbed layers with high rigidity and high modulus of elasticity, meaning that the carboxylic acid strongly bonds to the metal surface (Khanmohammadi et al., 2020). The thin oxide film and the strongly adsorbed layer act as a barrier hindering further tribofilm growth, resulting in low and steady friction throughout the test.

On the other hand, the friction mechanism of ILs is controlled by tribofilm formation, which depends on the electrical conductivity and the pH of the media. Both PP and BMP bring the same level of electrical conductivity to the base lubricant, but different pH having an effect on the tribofilm build up process. In the case of WG-BMP, due to the neutral pH, the presence of mainly iron oxides in the tribofilm was favoured,

in accordance with XPS results (Table 4). The tribofilm growth occurs via mechanical and chemical deposition, as shown in the STEM image for WG-BMP 100 m (Figure 5). The tribofilm growth influences the friction evolution (Figure 1), in which there is an increase of friction at the beginning of the test. The friction remains at high values for ca. 150 m when a thick tribofilm is present on the surface, and it reduces as the tribofilm is removed at the last 150 m of the test (Figure 1). In WG-PP, due to the high electrical conductivity, the tribofilm also grows. However, due to the low pH, more active dissolution (Fe^{2+}) occurs, and competition between tribofilm growth and active dissolution takes place. At the first 40 m of the sliding test, active dissolution overcomes the tribofilm growth, resulting in decreased friction (Figure 1). However, phosphorus (in the form of iron phosphate) in the tribofilm (Figure 5) stabilizes the tribofilm growth for the rest of the test. This allows for keeping a steady friction evolution. However, the friction values are higher than for C12 since the tribofilm is more rigid than the adsorbed carboxylic acid layer.

The Effect of Tribofilm on Wear

The additives resulted in a lower wear rate than the neat base lubricant (Figure 1), showing the additives' importance in the antiwear performance. As stated in Section 2.2, the wear rate was calculated based on the total volume loss occurring during the whole test. To further study the wear mechanism, a more detailed analysis of the volume loss was conducted. Wear profiles from each lubricant condition (Figure 7A) show the formation of ridges and a groove. Based on these 2-D wear profiles, the actual volume loss (area loss in this case) can be calculated from the difference between the groove and the ridges. The ridges area (A_{ridges}), groove area (A_{groove}), and area loss (ΔA) are presented in Figure 7B along with the degree of material loss (β). The measured areas are normalized to 100 m for easier comparison. The degree of material loss is defined as the ratio between area loss and groove area as shown in the following equation (Bruce, 2012):



$$\beta = \frac{A_{groove} - A_{ridges}}{A_{groove}} \times 100 = \frac{\Delta A}{A_{groove}} \times 100$$

β can be used as an indication of the type of wear, in which higher β indicates more abrasive wear whereas lower β indicates more plastic deformation.

Figure 7B shows that WG 300 m, WG-C12 300 m, and WG-BMP 300 m samples have comparable β values, indicating a similar wear mechanism, which corresponds to predominantly abrasive wear. However, the β values of WG-PP 300 m and WG-BMP 100 m are the lowest, indicating predominantly plastic deformation. This discrepancy in wear mechanisms is in agreement with the differences in tribofilm formation.

As shown from the STEM images and the EDS data (**Figure 5** and **Table 3**), WG-PP 300 m and WG-BMP 100 m produced a very thick tribofilms with the highest degree of oxidation. Indeed, the degree of oxidation is well correlated with the lower area loss (ΔA). This was also observed for the WG-BMP samples in which WG-BMP 100 m sample shows lower area loss (ΔA) than WG-BMP 300 m. The high electrical conductivity (i.e. oxidation degree) creates a thick tribofilm that reduces wear. Moreover, the WG-PP 300 m tribofilm also contains iron phosphate (**Figure 6** and **Table 5**), enhancing its antiwear properties. Therefore, the formation of a thick tribofilm has a beneficial effect on the wear reduction of the steel.

However, when looking at the wear track surface and the FIB cross-sections, the thickest tribofilms (WG-PP and WG-BMP 100 m) have poor adhesion to the metal (**Figure 2, 3, 4**) that can have a detrimental effect on the tribofilm integrity. The different mechanical properties of the tribofilm and the metal might be responsible for this behaviour, where under pressure, the ductile metal tends to plastically deform leading to cracking and detachment of the more brittle oxide tribofilm at the interface.

5 CONCLUSION

The effect of lubricant additive chemistry on friction and wear of AISI 52100 steel was investigated in a water-based lubricant. The following conclusions can be drawn:

- Dodecanoic acid showed a significant reduction in friction due to the adsorption on the metal surface. However, the oxide film growth was limited due to lower electrical conductivity, leading to higher wear rates.

REFERENCES

- Amiril, S. A. S., Rahim, E. A., and Syahrullail, S. (2017). A Review on Ionic Liquids as Sustainable Lubricants in Manufacturing and Engineering: Recent Research, Performance, and Applications. *J. Clean. Prod.* 168, 1571–1589. doi:10.1016/j.jclepro.2017.03.197
- Archard, J. F. (1953). Contact and Rubbing of Flat Surfaces. *J. Appl. Phys.* 24, 981–988. doi:10.1063/1.1721448
- Bernat, S., Armada, S., and Espallargas, N. (2018). Effect of Contamination on the Friction and Wear of Carboxylic Acids in Aqueous Lubricants. *Tribology Lett.* 66, 1–12. doi:10.1007/s11249-018-1116-9

- The ionic liquids investigated in this work increase the lubricant's electrical conductivity affecting the oxidation degree of the metal and the tribofilm formation. The resulting very thick tribofilms (400–1,300 nm) decrease the wear rate of the steel. However, these thick tribofilms do not significantly decrease friction.
- Ionic liquids influence the pH of the lubricant and therefore affect the chemical composition of the tribofilm, yielding different tribological responses. Lower pH generates more iron dissolution resulting in friction reduction due to the formation of iron phosphate.
- Iron phosphate stabilizes the tribofilm growth and provides it with better mechanical properties, being the effect more positive for wear than for friction.
- Thick and rigid tribofilms on the ductile base metal are brittle and promote crack formation at the interface, resulting in detachment and debris formation.

DATA AVAILABILITY STATEMENT

The original contributions presented in the study are included in the article/supplementary material, further inquiries can be directed to the corresponding authors.

AUTHOR CONTRIBUTIONS

WW planned and carried out the experiments, analyzed the data and wrote the manuscript. HK contributed to the design and implementation of the research, to the analysis of the results and to the writing of the manuscript. NE conceived the original idea of the research, was in charge of overall direction and planning the study and was the project supervisor. All authors discussed the results and commented on the manuscript.

ACKNOWLEDGMENTS

The authors would like to acknowledge the financial support from Indonesia Endowment Fund for Education (LPDP), M-ERA.NET GreenCOAT project with Project Number 4153, and the Norwegian Micro- and Nano-fabrication facility, NorFab, for providing the characterization facilities.

- Bernat, S., Armada, S., and Espallargas, N. (2018). Friction Mechanisms by Carboxylic Acids in Aqueous Lubricants. *Tribology Lett.* 66, 1–15. doi:10.1007/s11249-018-1035-9
- Bruce, R. W. (2012). *Handbook of Lubrication and Tribology, Volume II: Theory and Design*. Boca Raton: CRC Press.
- Candelaria, K. (2018). Finding Alternatives to ZDDP. Available at: https://www.lubesngreases.com/magazine/24_11/finding-alternatives-to-zddp/ (Accessed December 12, 2021).
- Canter, N. (2019). Special Report: ZDDP's Uncertain Future. Available at: https://www.stle.org/files/TLTArchives/2019/09_September/Tech_Beat.aspx (Accessed December 12, 2021).
- Chang, Z. Y., Breeden, D., and McDonald, M. (2011). The Use of Zinc Dialkyl Dithiophosphate as a Lubricant Enhancer for Drilling Fluids Particularly

- Silicate-Based Drilling Fluids. *Proc. - SPE Int. Symp. Oilfield Chem.* 2, 587–593. doi:10.2118/141327-ms
- Chen, Y., Jha, S., Raut, A., Zhang, W., and Liang, H. (2020). Performance Characteristics of Lubricants in Electric and Hybrid Vehicles: A Review of Current and Future Needs. *Front. Mech. Eng.* 6, 1–19. doi:10.3389/fmech.2020.571464
- Dong, R., Yu, Q., Bai, Y., Wu, Y., Ma, Z., Zhang, J., et al. (2020). Towards superior Lubricity and Anticorrosion Performances of Proton-Type Ionic Liquids Additives for Water-Based Lubricating Fluids. *Chem. Eng. J.* 383, 123201. doi:10.1016/j.cej.2019.123201
- Espallargas, N., Torres, C., and Muñoz, A. I. (2015). A Metal Ion Release Study of CoCrMo Exposed to Corrosion and Tribocorrosion Conditions in Simulated Body Fluids. *Wear* 332–333, 669–678. doi:10.1016/j.wear.2014.12.030
- European Environment Agency (2019). CO2 Emissions from Cars: Facts and Figures. Available at: <https://www.europarl.europa.eu/news/en/headlines/society/20190313STO31218/co2-emissions-from-cars-facts-and-figures-infographics> (Accessed December 12, 2021).
- Fontana, M. G. (1987). *Corrosion Engineering*. New York (USA): McGraw-Hill.
- Fredriksson, W., Malmgren, S., Gustafsson, T., Gorgoi, M., and Edström, K. (2012). Full Depth Profile of Passive Films on 316L Stainless Steel Based on High Resolution HAXPES in Combination with ARXPS. *Appl. Surf. Sci.* 258, 5790–5797. doi:10.1016/j.apsusc.2012.02.099
- Holmberg, K., and Erdemir, A. (2019). The Impact of Tribology on Energy Use and CO2 Emission Globally and in Combustion Engine and Electric Cars. *Tribology Int.* 135, 389–396. doi:10.1016/j.triboint.2019.03.024
- Huang, J., Zhou, X., Wang, J., Tang, X., and Kuang, F. (2019). Influence of Temperature on Friction of Polymeric Materials in Water. *Wear* 426–427, 868–876. doi:10.1016/j.wear.2019.01.115
- Jacobson, S., and Hogmark, S. (2010). “Tribofilms – On the Crucial Importance of Tribologically Induced Surface Modifications,” in *Recent Developments in Wear Prevention, Friction and Lubrication*. Editor G K Nikas (Kerala, India: Research Signpost), 661, 197–225.
- Kapsa, P., and Martin, J. M. (1982). Boundary Lubricant Films: A Review. *Tribology Int.* 15, 37–42. doi:10.1016/0301-679x(82)90110-4
- Khan, T., Broderick, M., and Taylor, C. M. (2021). Investigating the Industrial Impact of Hydraulic Oil Contamination on Tool Wear during Machining and the Development of a Novel Quantification Methodology. *Int. J. Adv. Manuf. Technol.* 112, 589–600. doi:10.1007/s00170-020-06370-y
- Khanmohammadi, H., Wijanarko, W., and Espallargas, N. (2020). Ionic Liquids as Additives in Water-Based Lubricants: From Surface Adsorption to Tribofilm Formation. *Tribol Lett.* 68, 130. doi:10.1007/s11249-020-01377-8
- Liu, W., Ye, C., Gong, Q., Wang, H., and Wang, P. (2002). Tribological Performance of Room-Temperature Ionic Liquids as Lubricant. *Tribology Lett.* 13, 81–85. doi:10.1023/a:1020148514877
- Long, Y., Bouchet, M. B., Lubrecht, T., Onodera, T., and Martin, J. M. (2019). Superlubricity of Glycerol by Self-Sustained Chemical Polishing. *Sci. Rep.* 9, 1–13. doi:10.1038/s41598-019-42730-9
- Minami, I. (2009). Ionic Liquids in Tribology. *Molecules* 14, 2286–2305. doi:10.3390/molecules14062286
- Morina, A., and Neville, A. (2007). Tribofilms: Aspects of Formation, Stability and Removal. *J. Phys. D: Appl. Phys.* 40, 5476–5487. doi:10.1088/0022-3727/40/18/s08
- Narita, K., and Takekawa, D. (2019). Lubricants Technology Applied to Transmissions in Hybrid Electric Vehicles and Electric Vehicles. SAE Technical Papers.
- Nicholls, M. A., Do, T., Norton, P. R., Kasrai, M., and Bancroft, G. M. (2005). Review of the Lubrication of Metallic Surfaces by Zinc Dialkyl-Dithiophosphates. *Tribology Int.* 38, 15–39. doi:10.1016/j.triboint.2004.05.009
- Phillips, B. S., and Zabinski, J. S. (2004). Ionic Liquid Lubrication Effects on Ceramics in a Water Environment. *Tribology Lett.* 17, 533–541. doi:10.1023/b:tril.0000044501.64351.68
- Rokosz, K., Hryniewicz, T., Simon, F., and Rzdakiewicz, S. (2016). Comparative XPS analyses of passive layers composition formed on Duplex 2205 SS after standard and high-current-density electropolishing. *Tehnicki Vjesnik* 23, 731–735. doi:10.17559/TV-20141107094438
- Seddon, K. R. (1997). Ionic Liquids for Clean Technology. *J. Chem. Technol. Biotechnol.* 68, 351–356. doi:10.1002/(sici)1097-4660(199704)68:4<351:aid-jctb613>3.0.co;2-4
- Somers, A., Howlett, P., MacFarlane, D., and Forsyth, M. (2013). A Review of Ionic Liquid Lubricants. *Lubricants* 1, 3–21. doi:10.3390/lubricants1010003
- Spikes, H. (2004). The History and Mechanisms of ZDDP. *Tribology Lett.* 17, 469–489. doi:10.1023/b:tril.0000044495.26882.b5
- Spikes, H. (2008). Low- and Zero-Sulphated Ash, Phosphorus and sulphur Anti-wear Additives for Engine Oils. *Lubrication Sci.* 20, 103–136. doi:10.1002/ls.57
- Spikes, H. (2015). Friction Modifier Additives. *Tribology Lett.* 60, 1–26. doi:10.1007/s11249-015-0589-z
- Stachowiak, G. W., and Batchelor, A. W. (2014). *Engineering Tribology*. Oxford (UK): Elsevier.
- THE EUROPEAN COMMISSION (2014). *Commission Regulation (EU) No 136/2014*. Brussel, Belgium: Official Journal of the European Union.
- Tomala, A., Karpinska, A., Werner, W. S. M., Olver, A., and Störi, H. (2010). Tribological Properties of Additives for Water-Based Lubricants. *Wear* 269, 804–810. doi:10.1016/j.wear.2010.08.008
- Transport and Environment (2019). *Electric Surge: Carmakers' Electric Car Plans across Europe 2019-2025*. Available at: <https://www.transportenvironment.org/discover/electric-surge-carmakers-electric-car-plans-across-europe-2019-2025/> (Accessed December 12, 2021).
- Urtis, L. A., Arcifa, A., Zhang, P., Du, J., Fantauzzi, M., Rauber, D., et al. (2019). Influence of Water on Tribolayer Growth when Lubricating Steel with a Fluorinated Phosphonium Dicyanamide Ionic Liquid. *Lubricants* 7, 27. doi:10.3390/lubricants7030027
- Van Rensselaar, J. (2019). The Tribology of Electric Vehicles. *Tribology Lubrication Technol.* 75, 34–43.
- Viesca, J. L., García, A., Hernández Batez, A., González, R., Monge, R., Fernández-González, A., et al. (2013). FAP– Anion Ionic Liquids Used in the Lubrication of a Steel-Steel Contact. *Tribol Lett.* 52, 431–437. doi:10.1007/s11249-013-0226-7
- Wang, Y., Yu, Q., Cai, M., Zhou, F., and Liu, W. (2018). Halide-Free PN Ionic Liquids Surfactants as Additives for Enhancing Tribological Performance of Water-Based Liquid. *Tribology Int.* 128, 190–196. doi:10.1016/j.triboint.2018.07.018
- Wasserscheid, P., and Welton, T. (2002). *Ionic Liquids in Synthesis*. Weinheim (Germany): Wiley-VCH Verlag GmbH & Co. KGaA.
- Welton, T. (1999). Room-Temperature Ionic Liquids. Solvents for Synthesis and Catalysis. *Chem. Rev.* 99, 2071–2084. doi:10.1021/cr980032t
- Welton, T. (2018). Ionic Liquids: A Brief History. *Biophys. Rev.* 10, 691–706. doi:10.1007/s12551-018-0419-2
- Xiao, H. (2017). Ionic Liquid Lubricants: Basics and Applications. *Tribology Trans.* 60, 20–30. doi:10.1080/10402004.2016.1142629
- Xie, G., Liu, S., Guo, D., Wang, Q., and Luo, J. (2009). Investigation of the Running-In Process and Friction Coefficient under the Lubrication of Ionic Liquid/Water Mixture. *Appl. Surf. Sci.* 255, 6408–6414. doi:10.1016/j.apsusc.2009.02.029
- Ye, C., Liu, W., Chen, Y., and Yu, L. (2001). Room-Temperature Ionic Liquids: A Novel Versatile Lubricant. *Chem. Commun.* 21, 2244–2245. doi:10.1039/b106935g
- Yu, B., Zhou, F., Pang, C., Wang, B., Liang, Y., and Liu, W. (2008). Tribological Evaluation of α , -diimidazoliumalkylene Hexafluorophosphate Ionic Liquid and Benzotriazole as Additive. *Tribology Int.* 41, 797–801. doi:10.1016/j.triboint.2008.02.004
- Zavieh, A. H., and Espallargas, N. (2017). The Effect of Friction Modifiers on Tribocorrosion and Tribocorrosion-Fatigue of Austenitic Stainless Steel. *Tribology Int.* 111, 138–147. doi:10.1016/j.triboint.2017.03.008
- Zheng, G., Zhang, G., Ding, T., Xiang, X., Li, F., Ren, T., et al. (2017). Tribological Properties and Surface Interaction of Novel Water-Soluble Ionic Liquid in Water-Glycol. *Tribology Int.* 116, 440–448. doi:10.1016/j.triboint.2017.08.001
- Zhou, Y., and Qu, J. (2017). Ionic Liquids as Lubricant Additives: A Review. *ACS Appl. Mater. Inter.* 9, 3209–3222. doi:10.1021/acsami.6b12489
- Zhou, Y., Leonard, D. N., Guo, W., and Qu, J. (2017). Understanding Tribofilm Formation Mechanisms in Ionic Liquid Lubrication. *Sci. Rep.* 7, 8426–8428. doi:10.1038/s41598-017-09029-z

Conflict of Interest: The authors declare that the research was conducted in the absence of any commercial or financial relationships that could be construed as a potential conflict of interest.

Publisher's Note: All claims expressed in this article are solely those of the authors and do not necessarily represent those of their affiliated organizations, or those of the publisher, the editors and the reviewers. Any product that may be evaluated in this article, or claim that may be made by its manufacturer, is not guaranteed or endorsed by the publisher.

Copyright © 2022 Wijanarko, Khanmohammadi and Espallargas. This is an open-access article distributed under the terms of the Creative Commons Attribution License (CC BY). The use, distribution or reproduction in other forums is permitted, provided the original author(s) and the copyright owner(s) are credited and that the original publication in this journal is cited, in accordance with accepted academic practice. No use, distribution or reproduction is permitted which does not comply with these terms.